Solid Earth, 12, 2145–2157, 2021
https://doi.org/10.5194/se-12-2145-2021

Solid Earth Open Access EGU

Dating folding beyond folding, from layer-parallel shortening to fold tightening, using mesostructures: lessons from the Apennines, Pyrenees, and Rocky Mountains

Olivier Lacombe[1], Nicolas E. Beaudoin[2], Guilhem Hoareau[2], Aurélie Labeur[2], Christophe Pecheyran[3], and Jean-Paul Callot[2]

[1]Institut des Sciences de la Terre de Paris, Sorbonne Université, CNRS, Paris, France
[2]Laboratoire des Fluides Complexes et de leurs Réservoirs, Universite de Pau et des Pays de l'Adour, E2S UPPA, CNRS-TOTAL, Pau, France
[3]Institut des Sciences Analytiques et de Physico-Chimie pour l'Environnement et les Matériaux, Universite de Pau et des Pays de l'Adour, E2S UPPA, Pau, France

Correspondence: Olivier Lacombe (olivier.lacombe@sorbonne-universite.fr)

Received: 18 June 2021 – Discussion started: 23 June 2021
Revised: 26 August 2021 – Accepted: 6 September 2021 – Published: 30 September 2021

Abstract. Dating syntectonic sedimentary sequences is often seen as the unique way to constrain the initiation, duration, and rate of folding as well as the sequence of deformation in the shallow crust. Beyond fold growth, however, deformation mesostructures accommodate the internal strain of pre-folding strata before, during, and after strata tilting. Absolute dating of syn-folding mesostructures may help constrain the duration of fold growth in the absence of preserved growth strata. Absolute dating of mesostructures related to early-folding layer-parallel shortening and late fold tightening provides an access to the timing and duration of the entire folding event. We compile available ages from the literature and provide new U–Pb ages of calcite cements from veins and faults from four folds (Apennines, Pyrenees, Rocky Mountains). Our results not only better constrain the timing of fold growth but also reveal a contraction preceding and following folding, the duration of which might be a function of the tectonic style and regional sequence of deformation. This study paves the way for a better appraisal of folding lifetime and processes and stress evolution in folded domains.

1 Introduction

Quantifying the rates and duration of deformation processes is key to understanding how the continental crust deforms. Quite a lot is known about rates and duration of ductile deformation in the lower crust, for instance that shear zones can be active for tens to hundreds of millions of years (Schneider et al., 2013; Mottram et al., 2015). However, less is known about the duration and rates of folding processes in the upper crust. Short-term folding rates are usually captured by studying deformed terraces and alluvial fan ridges associated with active folds, and the dating of the inception and lifetime of folds is based on the extrapolation of these short-term rates back in time assuming a steady deformation rate.

The other classical means of constraining the age and rate of upper-crustal folding consists of dating growth strata. In orogenic forelands, contractional deformation causes folding of the pre-deformational sedimentary sequence, and when sedimentation occurs continuously during deformation, growth strata are deposited synchronously with folding. Growth strata often show a characteristic pattern, such as decreasing dips up-section toward the limbs of the fold, fan-like geometry, and unconformities (Riba, 1976; Fig. 1). Several factors control growth strata patterns, such as kink-band migration, fold uplift, limb rotation and lengthening rates, as well as sedimentation and erosion rates (Suppe et al., 1992; Storti and Poblet, 1997). Chronostratigraphic constraints are

critical for defining the duration and rate of fold growth (Butler and Lickorish, 1997). Dating the base of the growth strata defines the youngest initiation age for the fold, while post-growth strata conceal the final geometry of the fold and mark the end of folding (Fig. 1).

However, preserved growth strata are not ubiquitous/are rare, and the folded multilayer typically includes only pre-growth strata. Also, the fold growth may be highly discontinuous through time, deformation being episodic at all timescales with tectonic uplift pulses of different duration and intensity interrupted by periods of variable extent in which no fold growth occurred (Masaferro et al., 2002; Carrigan et al., 2016; Anastasio et al., 2017). Where available, the study of syntectonic unconformities (Barnes, 1996) or terraces (Mueller and Suppe, 1997) otherwise suggests that the growth of some folds may be caused by earthquake-related slip on active faults, which is by its nature discontinuous. These studies emphasize the difficulty in extrapolating fold growth rates back in time. The age of fold initiation obtained by assuming steady shortening, deposition, and fold growth rates is therefore at best strongly biased and at worst false, so the duration of fold growth remains poorly constrained.

Folded sedimentary layers usually exhibit brittle mesostructures such as faults, joints, veins, and stylolites (e.g. Tavani et al., 2015, and references therein). These mesostructures accommodate the internal strain of strata during folding but also before strata started to be tilted and after tilting, i.e. when shortening can no longer be accommodated by fold growth (Fig. 1). Several deformation stages can typically be identified in folded pre-compressional strata, starting with pre-shortening extension related to foreland flexure and bulging, followed by layer-parallel shortening (LPS, horizontal shortening of flat-lying strata) (Amrouch et al., 2010a; Callot et al., 2010; Lacombe et al., 2011; Tavani et al., 2006, 2008, 2011, 2012; Rocher et al., 2000; Beaudoin et al., 2012, 2016; Branellec et al., 2015). Continuing horizontal stress loading and shortening usually leads to folding, associated with strata tilting and curvature, which are accommodated by flexural slip in the fold limbs and tangential longitudinal strain (outer-arc extension and inner-arc compression) at the fold hinge. The fold "locks" when limb rotation and/or kink-band migration cannot accommodate shortening anymore. At that stage, strata tilting is over but continuous horizontal shortening leads to late-stage fold tightening (LSFT), accommodated by late mesostructures developing irrespective of bedding dip (Fig. 1) (Amrouch et al., 2010a; Tavani et al., 2015).

Despite recent efforts (Wang et al., 2016; Grobe et al., 2019; Curzi et al., 2020; Cruset et al., 2020, 2021), the dating of the early-, syn-, and late-folding mesostructures has received poor attention, although it is key to constraining not only the absolute timing of folding in the absence of growth strata but also the entire duration of the fold-related contractional stages and the associated stress evolution from build-up to release. We explore hereinafter the possibility to define the age and duration of folding by investigating how and for how long pre-folding strata have been accommodating shortening from the onset to the end of the horizontal contraction from which the fold originated, an event we define as the folding event (Fig. 1). This approach will help better constrain the duration of fold growth, by directly dating the syn-folding mesostructures but also by bracketing the timing of fold growth through the dating of the mesostructures that immediately predate and postdate strata tilting. Doing so will also enable us to capture the duration of the LPS and LSFT. These two deformation stages have been overlooked since they accommodate much less shortening than folding itself. However, they correspond to key periods of time for large-scale fluid flow and related ore deposition in fold-and-thrust belts and sedimentary basins (e.g. Roure et al., 2005; Evans and Fischer, 2012; Beaudoin et al., 2014). For this purpose, we consider four natural folds for which we either compile existing data or provide new estimates of the age of LPS, fold growth, and LSFT. Three of our examples are from fold-and-thrust belts (Apennines, Pyrenees) and one from the Laramide basement-cored folding province (Rocky Mountains). We show that mesostructures can be used to constrain the timing and duration of fold growth and/or of shortening preceding and following folding. Our results not only provide new estimates of the duration of folding but also establish that the overall duration of the folding event may strongly vary as a function of the tectonic style of deformation. Beyond regional implications, this study paves the way to a better mechanical appraisal of contractional deformation and stress evolution in folded domains.

2 Methods for dating the folding event using mesostructures

In this paper, we focus on easily recognizable mesostructures that develop in the same contractional stage and under the same regional trend of horizontal shortening as folding. We report neither on microstructures such as calcite twins (Craddock et al., 1993; Lacombe et al., 2007, 2009; Rocher et al., 1996; Hnat et al., 2011; see review by Lacombe, 2010) nor on rock physical properties such as anisotropy of magnetic susceptibility (e.g. Aubourg et al., 2010; Amrouch et al., 2010b; Branellec et al., 2015; Weil and Yonkee, 2012). The main reason is that although both of them have been shown to be suitable recorders of the stress and strain history of folded strata (Lacombe et al., 2012), their precise dating remains out of reach to date.

In the four folds that we investigated, the sequence and age of mesostructures were established by various dating approaches, the methodologies of which are briefly recalled below (Fig. 2). Note that strata from which mesostructures were dated are mainly pre-folding strata and that there have been few (if any) attempts at directly dating mesostructures that developed within growth strata. The reason is that the of-

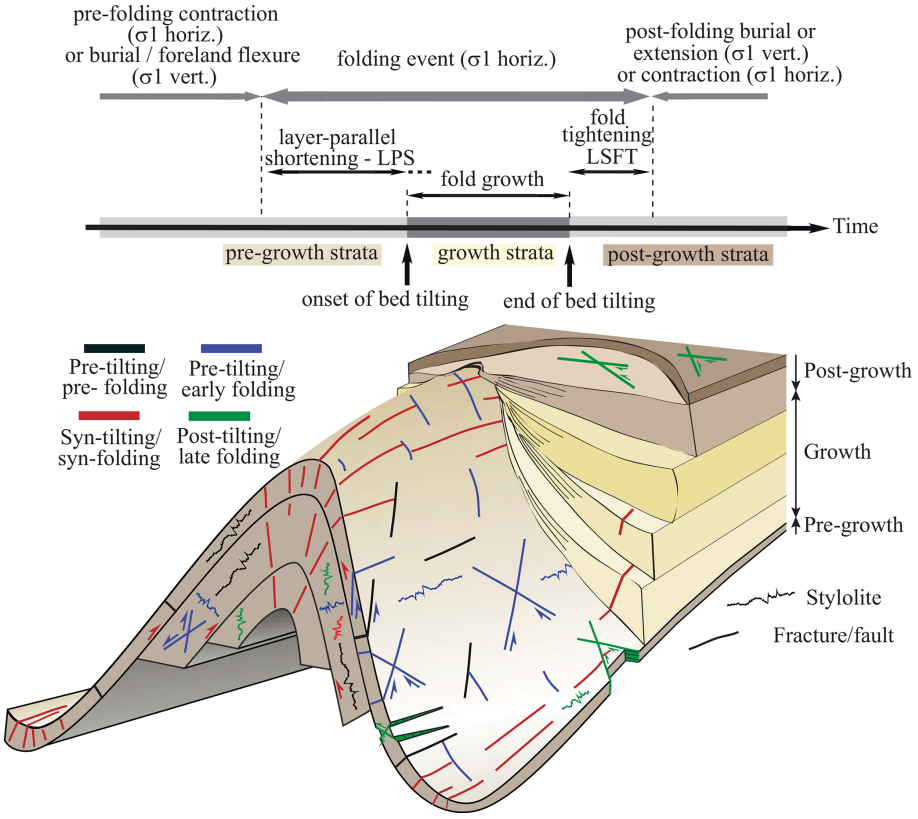

Figure 1. Concept of folding event and associated mesostructures and growth strata.

ten poorly indurated syn-folding formations are less prone to fracturing and calcite cementation at the time of deformation compared to pre-folding, well-indurated formations, which is evidenced by the paucity of fracture studies in syntectonic strata (e.g. Shackleton et al., 2011).

2.1 Sequence of mesostructures related to the fold history

The characterization of the sequence of deformation was based on field measurements of stylolites, faults, joints, and veins and their grouping into sets according to their statistical orientation, deformation mode, and relative chronology established from abutting and crosscutting relationships (Fig. 2a). Their timing with respect to fold growth (i.e. early-, syn-, and late-folding mesostructures) was further established by considering their current and unfolded attitude at the fold hinge and limbs (e.g. Beaudoin et al., 2012, 2016; Tavani et al., 2015) (Fig. 1).

Field observations (e.g. Bellahsen et al., 2006; Ahmadhadi et al., 2008; Tavani et al., 2015) and numerical modelling (Guiton et al., 2003; Sassi et al., 2012) have emphasized the widespread reactivation during folding of joints and veins formed during pre-folding stages. The role of reactivation should not be, and has not been, overlooked in our study; however, for the sake of reliable absolute dating we focused on faults and veins the characteristics of which support that they newly formed at each deformation stage and show neither textural nor petrographic evidence of multiple opening or shearing events, be it at the mesoscale or at the microscale.

2.2 Dating veins and faults

Calcite-bearing veins and faults (Fig. 2a) can be dated by combining the absolute precipitation temperature of the fluids from which calcite cements formed as given by carbonate clumped isotope Δ_{47} thermometry with the burial-time history of strata (Fig. 2b and d). Provided that (1) cementation was nearly coeval with fracturing, (2) the geotherm can be reliably estimated, and (3) stable isotope geochemistry points to fluid precipitation at thermal equilibrium with the host rock, clumped isotope thermometry of cements combined with strata burial history yields the absolute timing of the successive vein sets and hence the timing of the related deformation stages (Fig. 2d) (Labeur et al., 2021).

Calcite cements can also be directly dated by carbonate geochronology (Fig. 2b). Laser-ablation–inductively-coupled-plasma–mass-spectrometry (LA-ICP-MS) U–Pb dating of calcite consistently reveals the age of brittle deformation events (Roberts and Walker, 2016; Nuriel et al., 2017; Hansman et al., 2018; Beaudoin et al., 2018; Roberts et al., 2020) (Fig. 2b and d), provided that cementation was

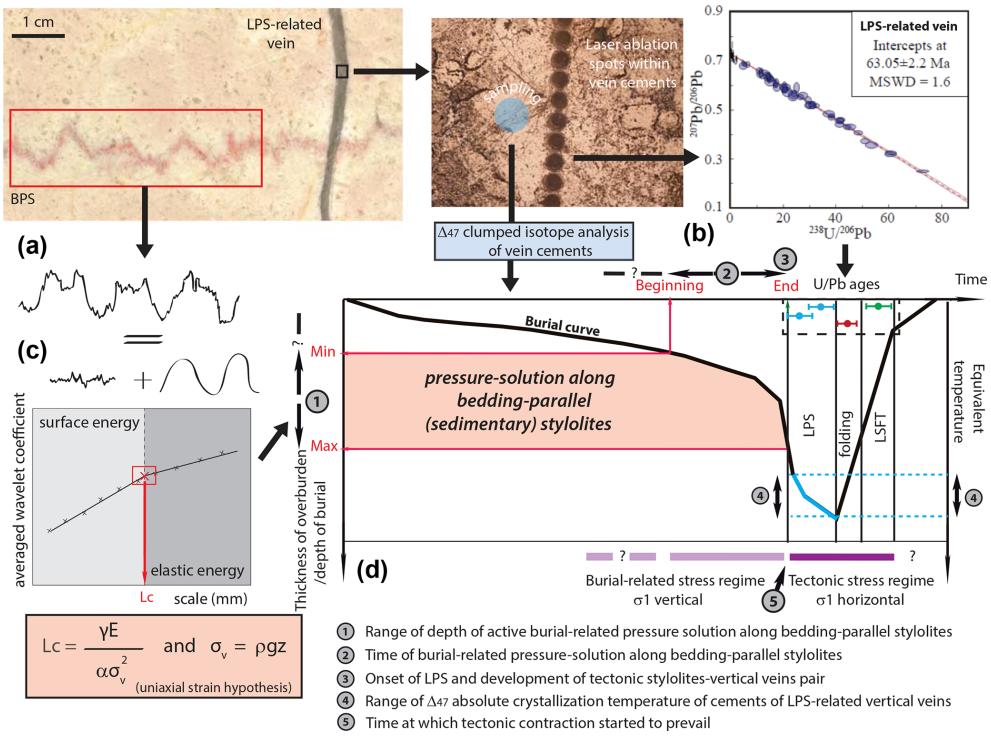

Figure 2. Principle of the dating of mesostructures related to the folding event. **(a)** Photograph of a bedding-parallel sedimentary stylolite cut by a vertical vein related to layer-parallel shortening (LPS). **(b)** Principle of dating calcite veins using LA-ICP-MS, with laser ablation spots and final Tera–Wasserburg diagram. **(c)** Principle of inversion of the roughness of sedimentary stylolites for stress. σ_v is the vertical stress, $\alpha = ((1-2\nu)\cdot(1+\nu)^2)/(30\pi(1-\nu)^2)$, γ is the solid–fluid interfacial energy, ν is the Poisson ratio, E is the Young modulus, ρ is the dry density, g is the gravitational field acceleration, and z is the depth. **(d)** Principle of the combination of U–Pb dating and absolute Δ_{47} thermometry of calcite cements (here for LPS-related veins) with maximum depth of burial-related dissolution inferred from roughness inversion of sedimentary stylolites and burial-time evolution of strata to derive the timing of deformation stages during the folding event.

coeval with fracturing and that no later fluid infiltration and/or calcite recrystallization occurred (Roberts et al., 2021).

2.3 Combining sedimentary stylolite roughness inversion for paleodepth and burial history to constrain the onset of LPS

The onset of LPS corresponds to the time at which the maximum principal stress $\sigma 1$ switched from a vertical attitude related to compaction and/or to foreland flexural extension to a horizontal attitude in response to tectonic contraction (Beaudoin et al., 2020a). In order to constrain the timing of this switch, our approach relies on the capability of bedding-parallel, sedimentary stylolite (Fig. 2a) to fossilize the magnitude of the vertical stress $\sigma 1$ at the time at which dissolution stopped. Indeed, signal analysis (e.g. wavelets) of the final roughness of a sedimentary stylolite returns scale-dependent power laws, of which the transition length (crossover length L_c) scales with the magnitude of the vertical stress $\sigma_v = \sigma 1$ (Schmittbuhl et al., 2004; Toussaint et al., 2018) (Fig. 2c). By analysing a population of sedimentary stylolites with this inversion technique, which has been validated by numerous studies (Ebner et al., 2009; Rolland et al., 2012, 2014; Bertotti et al., 2017; Beaudoin et al., 2016, 2019, 2020a, b), one can estimate the maximum burial depth at which pressure solution was active, with 12 % uncertainty (Rolland et al., 2014). Combining this depth with the burial-time evolution of the strata as derived from well data and/or exposed stratigraphic successions reveals the time at which compaction-driven pressure solution was halted in the rock because of the switch from a vertical to a horizontal $\sigma 1$ and thus the age of the onset of LPS (Fig. 2d). The validity of such an approach has been established on the basis of the comparison of the age of the onset of LPS determined this way with the oldest U–Pb absolute age of LPS-related veins (Beaudoin et al., 2020a).

3 Dating natural folding events

3.1 Cingoli and San Vicino Anticlines (Apennines)

The San Vicino and Cingoli anticlines belong to the Umbria–Marche Apennine Ridge (UMAR, Fig. 3a). Apenninic deformation occurred by the Tortonian in the west of UMAR to the

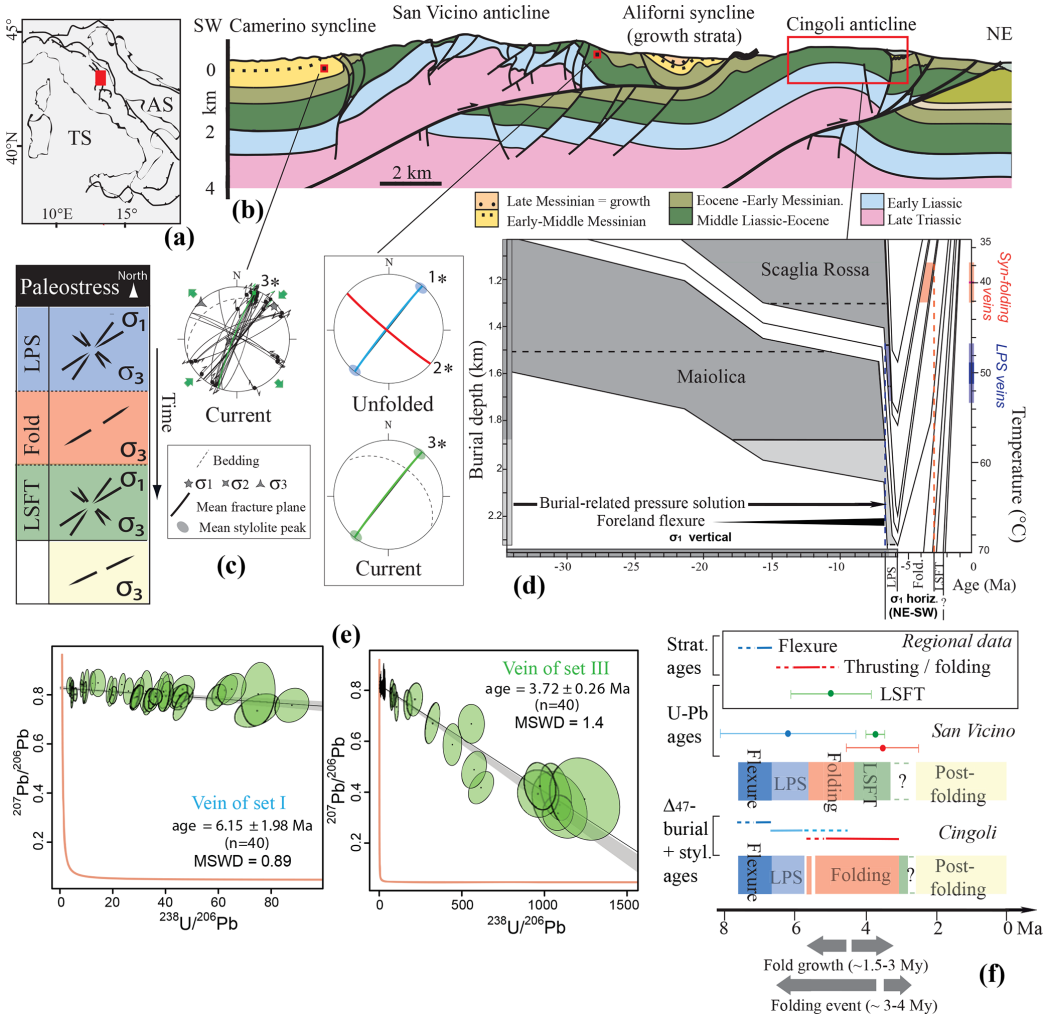

Figure 3. San Vicino and Cingoli anticlines. **(a)** Location (AS: Adriatic Sea; TS: Tyrrhenian Sea). **(b)** Cross section (modified after Mazzoli et al., 2002). **(c)** Orientation of the main sets of mesostructures (relative chronology, 1 to 3), reported in current or unfolded attitude on a lower-hemisphere Schmidt stereonet, and associated paleostress evolution; * denotes mesostructures dated using U–Pb. **(d)** Burial model of Cingoli constructed considering thickness from stratigraphic and well data corrected for chemical and physical compaction (modified after Labeur et al., 2021). The range of depths reconstructed from sedimentary stylolite roughness inversion (with uncertainty shaded in light grey) is reported for each formation as grey levels. The results of clumped isotope analysis (i.e. temperatures of precipitation of vein cements at thermal equilibrium with the host rock) are reported for LPS-related veins (blue) and syn-folding veins (red). The deduced timing of the deformation stages is reported. **(e)** Age dating results for veins from the San Vicino anticline: Tera–Wasserburg concordia plots for carbonate samples showing $^{238}U/^{206}Pb$ vs. $^{207}Pb/^{206}Pb$ for veins of sets I (LPS-related) and III (LSFT-related) (n – no. of spots). MSWD – mean square of weighted deviates. **(f)** Timing and duration of deformation stages. Regional data are from Mazzoli et al. (2002) (flexure), Calamita et al. (1994) (folding and thrusting), and Beaudoin et al. (2020b) (LSFT). Colour code for **(c, f)**: dark blue – flexure-related extension; blue – layer-parallel shortening (LPS); red – fold growth; green – late-stage fold tightening (LSFT); yellow – post-folding extension.

late Messinian–early Pliocene in the east, reaching the Adriatic domain in the late Pliocene–Pleistocene (Calamita et al., 1994). UMAR has been undergoing post-orogenic extension since ∼ 3 Ma, being younger eastward and marked by recent or active normal faults cutting through the nappe stack (Barchi, 2010). The San Vicino and the Cingoli anticlines involve platform carbonates overlain by a hemipelagic succession detached above Triassic evaporites. The folds formed in the late Messinian–early Pliocene (∼ 6–5 Ma) as indicated by growth strata preserved in the nearby Aliforni syncline (Fig. 3b), following a period of foreland flexure-related extension marked by pre-contractional normal faults associated with turbidite deposition lasting until the early Messinian (∼ 6.5 Ma) (Calamita et al., 1994; Mazzoli et al., 2002).

Field analysis in the Cingoli and San Vicino fault-bend anticlines (Fig. 3b) has revealed three main sets of mesostructures (Beaudoin et al., 2020b; Labeur et al., 2021). Set I consists of vertical veins perpendicular to both bedding and fold

axis and striking NE–SW, associated with bed-perpendicular tectonic stylolites with peaks trending NE–SW and plunging parallel to bedding dip which, after unfolding, indicates NE–SW-directed LPS. Set II veins are bed-perpendicular and strike NW–SE, parallel to the fold axis; they abut or cut across set I veins and formed in response to outer-arc extension at the fold hinge. Set III comprises NE–SW-striking veins closely associated with tectonic stylolites with horizontal peaks trending NE–SW – both veins and tectonic stylolites being vertical regardless of the bedding dip – and with conjugate vertical strike-slip faults which formed during a post-tilting horizontal NE–SW contraction, i.e. LSFT (Fig. 3c).

Labeur et al. (2021) focused on the Cingoli anticline to reconstruct the burial history of the early Cretaceous Maiolica Fm and the Paleocene Scaglia Rossa Fm. The authors carried out an extensive inversion of the roughness of sedimentary stylolites from these formations to constrain the maximum depth at which compaction-related dissolution was active. The results are shown in Fig. 3d, together with the timing of veins from sets I and II as deduced from Δ_{47} thermometry (Labeur et al., 2021) by considering a $23\,^{\circ}\mathrm{C\,km^{-1}}$ geotherm (Caricchi et al., 2015) and a 10 °C surface temperature. The resulting timing for LPS, fold growth, and LSFT is shown in Fig. 3f.

To extend the published dataset to the San Vicino Anticline, veins from sets I, II, and III were sampled in the Maiolica Fm to perform U–Pb analyses for absolute dating. Selected veins display antitaxial, elongated blocky, or blocky textures (Bons et al., 2012) ensuring that the cements precipitated during, or soon after, vein opening. Cathodoluminescence observations further support the homogeneity of the cements (Fig. 4) as well as the absence of any vein reopening and calcite recrystallization or fluid infiltration that might cause anomalous younger (reset) ages (Roberts et al., 2021). U–Pb dating of calcite cements was conducted using LA-ICP-MS at the Institut des Sciences Analytiques et de Physico-Chimie pour l'Environnement et les Matériaux (IPREM) laboratory (Pau, France). Ages were determined from the total-Pb/U–Th algorithm of Vermeesch (2020), are quoted at 95 % confidence, and include the propagation of systematic uncertainties. Sample information, a detailed methodology, and results are provided in the Supplement. Three veins from the San Vicino anticline yielded reliable ages: 6.1 ± 2 Ma for the set I vein, 3.5 ± 1 Ma for the set II vein, and 3.7 ± 0.3 Ma for the set III vein (Fig. 3e). The large uncertainties in the U–Pb age from the set II vein lead to some overlap with the dates of set I and set III veins (Fig. 3f). However, these veins have distinctive orientations, a consistent relative chronology, and distinctive C and O stable isotopic signatures of their cements while being sampled in the same parts of the fold (Beaudoin et al., 2020b). These observations support that these veins were not cemented by the same fluid and hence were not cemented coevally. The absolute vein ages, combined with existing time constraints

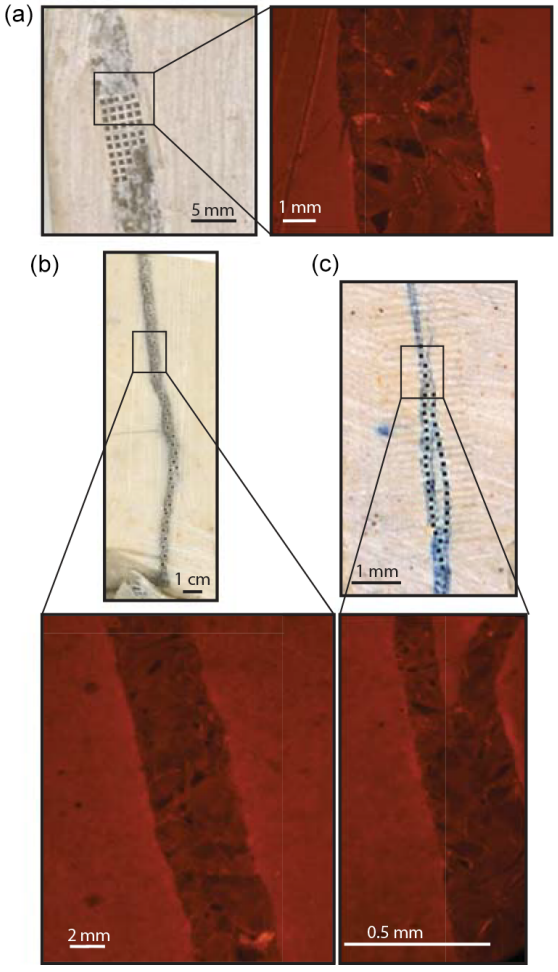

Figure 4. Two-dimensional scans of veins dated by LA-ICP-MS U–Pb geochronology from the San Vicino anticline, with the location of the ablation spots and diagenetic state observed under cathodoluminescence microscopy. **(a)** Sample A16 (LPS-related vein). **(b)** Sample A19 (syn-folding vein). **(c)** Sample A20 (LSFT-related vein).

(Fig. 3f), indicate that LPS occurred from ∼ 6.5 to 5.5 Ma for both anticlines, followed by fold growth between ∼ 5.5 and ∼ 3.5 Ma, with a seemingly slightly longer duration in Cingoli than in San Vicino. LSFT started ∼ 5 Ma in the Camerino syncline (Beaudoin et al., 2020b), ∼ 4.5 Ma in San Vicino, and ∼ 3 Ma in Cingoli and possibly lasted until the onset of post-orogenic extension in eastern UMAR (∼ 2.5–2 Ma, Fig. 3f). The entire folding event was thus very short, having lasted 3–4 Myr considering both anticlines as a whole (Fig. 3f).

3.2 Pico del Aguila Anticline (Pyrenees)

The Pico del Aguila is a N160° E-trending anticline in the southern Pyrenees (Fig. 5a), markedly oblique to the south Pyrenean thrust front. It formed in response to Pyrenean

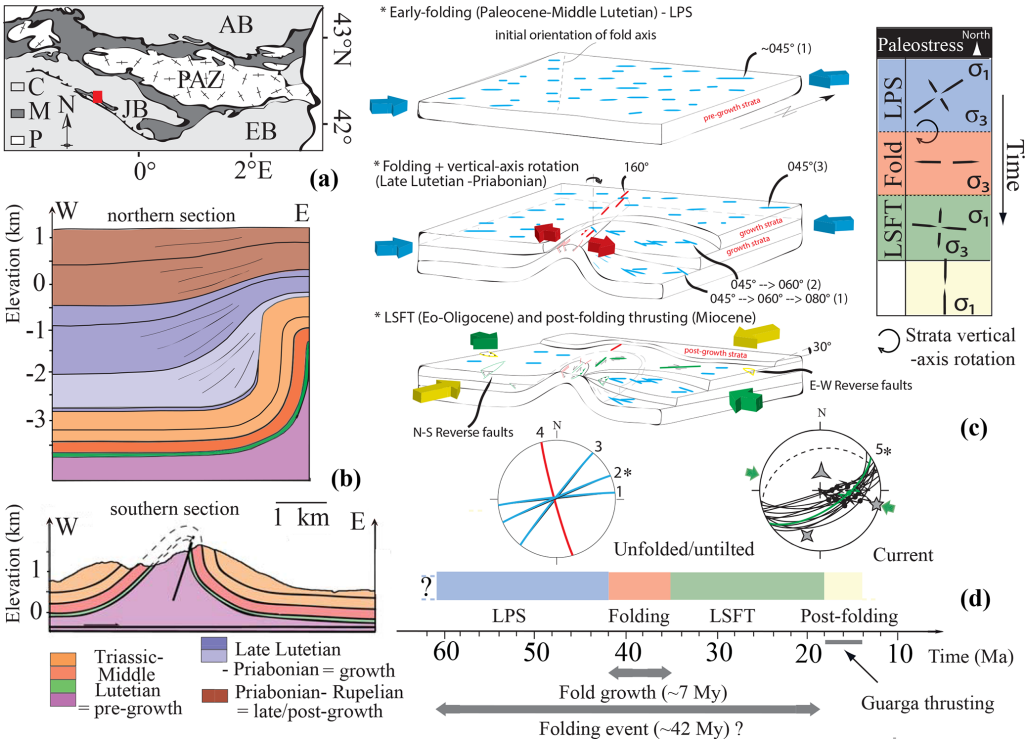

Figure 5. Pico del Aguila anticline. **(a)** Location (AB: Aquitaine Basin; JB: Jaca Basin; EB: Ebro Basin; PAZ: Pyrenean Axial Zone; P: Paleozoic; M: Mesozoic; C: Cenozoic). **(b)** Cross sections (north: modified after Poblet et al., 1997; south: modified after Beaudoin et al., 2015). **(c)** Orientation of the main sets of mesostructures (relative chronology, 1 to 5), reported in current or unfolded attitude on a lower-hemisphere Schmidt stereonet (same key as Fig. 3), and associated structural and paleostress evolution. Block diagrams modified after Beaudoin et al. (2015); * denotes mesostructures dated using U–Pb. **(d)** Timing and duration of deformation stages. Colour code for **(c, d)**: blue – layer-parallel shortening (LPS); red – fold growth; green – late-stage fold tightening (LSFT); yellow – post-folding compression.

thrusting and detachment folding above Triassic evaporites (Poblet and Hardy, 1995; Vidal Royo et al., 2009, Fig. 5b). Growth strata (Fig. 5b) indicate that the fold developed by the late Lutetian–Priabonian (∼ 42–35 Ma, Hogan and Burbank, 1996), before it was passively tilted and transported southward over the Guarga basement thrust (Jolivet et al., 2007).

Beaudoin et al. (2015) investigated the fracturing history of the Pico del Aguila (Fig. 5c). Three sets of bed-perpendicular joints/veins, oriented N080, N060, and N045° E (from the oldest to the youngest as established from abutting/cross-cutting relationships), were recognized. These three sets formed in progressively younging strata in response to a NE–SW-directed shortening while the area was undergoing a vertical axis 30–40° clockwise rotation (Fig. 5c). This rotation agrees with the Bartonian–Priabonian clockwise rotation of 15–50° around a vertical axis identified from paleomagnetism (Pueyo et al., 2002). The field study also revealed bed-perpendicular joints oriented N160° E and N–S-trending normal faults which formed during fold growth in response to outer-arc extension at the fold hinge (Fig. 5c). The end of the fold-related fracturing history (LSFT) is marked by the formation of N–S-trending reverse faults and by the transpressional reactivation of earlier ENE-striking joints under an E–W compression resulting from the local rotation of the regional NE–SW compression (Beaudoin et al., 2015). Post-folding, E–W-trending reverse faults ultimately developed under the same N–S compression as the Guarga thrust (Fig. 5c).

U–Pb dating of calcite cements reveals that the veins related to the NE–SW-directed LPS formed as early as ∼ 61 ± 3 Myr ago, while late oblique-slip reverse faults (LSFT) and post-folding E–W reverse faults were dated to 19 ± 5 and 18–14 ± 3 Ma, respectively (Hoareau et al., 2021). LPS, folding, and LSFT therefore lasted ∼ 19 Myr (61–42 Ma), ∼ 7 Myr (42–35 Ma), and ∼ 17 Myr (35–18 Ma), respectively (Fig. 5d).

3.3 Sheep Mountain Anticline (Rocky Mountains)

The Sheep Mountain anticline is a thrust-related, basement-cored NW–SE-striking fold that developed in the Bighorn basin (Fig. 6a and b) during the late Cretaceous–Paleogene Laramide contraction. Three main joint/vein sets were recognized there (Fig. 6c, Bellahsen et al., 2006; Amrouch et al., 2010a; Barbier et al., 2012). Set I consists of bed-perpendicular, WNW–ESE-oriented veins associated with tectonic stylolites with ∼WNW–ESE horizontal peaks (after

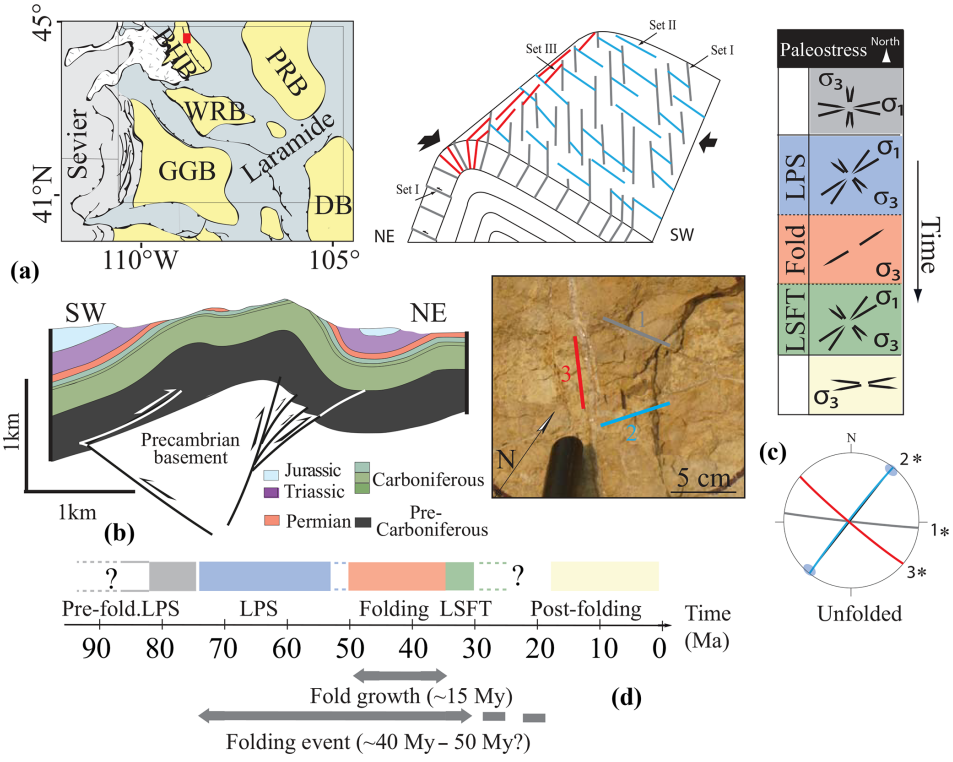

Figure 6. Sheep Mountain anticline. **(a)** Location (BHB: Bighorn basin; WRB: Wind River Basin; PRB: Powder River Basin; GGB: Greater Green River Basin; DB: Denver Basin). **(b)** Cross section (modified after Amrouch et al., 2010); **(c)** Orientation of the main sets of veins (relative chronology, 1 to 3), shown on a field photograph and on a block diagram of the final fold geometry, reported in unfolded attitude on a lower-hemisphere Schmidt stereonet (same key as Fig. 3), and associated structural and paleostress evolution; * denotes mesostructures dated using U–Pb. **(d)** Timing and duration of the deformation stages. Colour code for **(c, d)**: grey – pre-folding layer-parallel shortening kinematically unrelated to folding; blue – layer-parallel shortening (LPS); red – fold growth; green – late-stage fold tightening (LSFT); yellow – post-folding extension.

unfolding) (Amrouch et al., 2010a, 2011). This set formed prior to folding under a horizontal $\sigma 1$ trending WNW–ESE, likely transmitted from the distant thin-skinned Sevier orogen at the time the Bighorn basin was still part of the Sevier undeformed foreland. Set II comprises vertical, bed-perpendicular joints/veins striking NE–SW, i.e. perpendicular to the fold axis. These veins are associated with tectonic stylolites with horizontal peaks oriented NE–SW and witness a NE–SW-directed Laramide LPS (Varga, 1993; Amrouch et al., 2010a; Weil and Yonkee, 2012). The joints/veins of set III are bed-perpendicular and abut or cut across the veins of the former sets. They strike NW–SE, i.e. parallel to the fold axis, and their distribution mainly at the hinge zone of the fold supports their development in response to outer-arc extension at the hinge of the growing anticline (Fig. 6c). Widespread reverse and strike-slip faults also formed during LPS and LSFT, while bedding-parallel slip surfaces developed during fold growth (Amrouch et al., 2010a).

Veins from sets I, II, and III were dated by means of U–Pb (Beaudoin et al., 2018). Set I veins yielded ages between 81 and 72 Ma, supporting their pre-Laramide formation. The Laramide LPS-related veins were dated to 72–50 Ma. The age of set III veins constrains the timing of folding in the absence of preserved growth strata to 50–35 Ma (Beaudoin et al., 2018). Laramide LPS and fold growth therefore lasted ~ 20–25 Myr and ~ 15 Myr, respectively (Fig. 6d). The duration of the LSFT is poorly constrained, being bracketed between 35 Ma and the onset of the Basin and Range extension and Yellowstone hot-spot activity at ~ 17 Ma (Camp et al., 2015, Fig. 6d).

4 Discussion and conclusion

The absolute dating of mesostructures definitely confirms the sequence of deformation usually deduced from orientation data and relative chronology with respect to bedding attitude, which includes LPS, fold growth (e.g. strata tilting), and LSFT (Fig. 1). This sequence is valid for the four folds studied, despite the San Vicino, Cingoli and Pico del Aguila anticlines developed above a decollement in a fold-and-thrust belt, while the Sheep Mountain anticline formed as a basement-cored forced fold above a basement thrust. The overall consistency between the ages of growth strata when

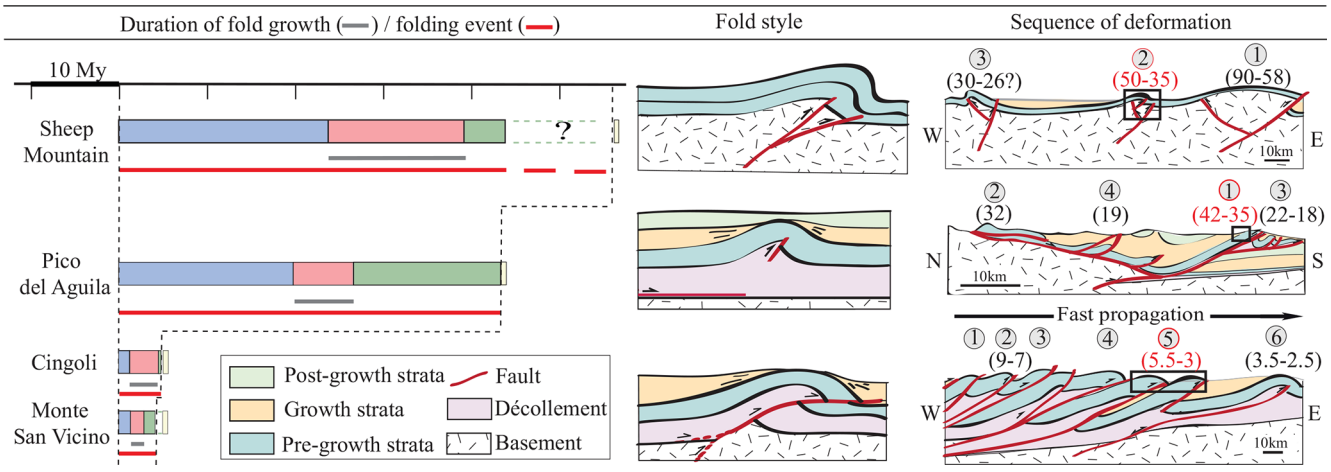

Figure 7. Compared durations of the deformation stages of the folding event, fold style (i.e. final fold geometry) and sequence of regional deformation for the four studied folds (circled numbers 1 to 6: order of structural development, i.e. sequence of folding/thrusting, with corresponding ages in Ma (in parentheses)); red: from this study; black: from the literature (Beaudoin et al., 2018, for Wyoming, Jolivet et al., 2007, for the Pyrenees, Calamita et al., 1994, and Curzi et al., 2020, for the Apennines). Colour code: blue – layer-parallel shortening (LPS); red – fold growth; green – late-stage fold tightening (LSFT); yellow – post-folding extension/compression.

preserved, the time constraints derived from our multi-proxy analysis coupling isotopic geochemistry of cements and stylolite paleopiezometry, and the U–Pb ages on early-, syn-, and late-folding mesostructures demonstrates the reliability of our approach. Minor age overlaps are observed only when the duration of each deformation stage was shorter than age uncertainties, i.e. in the case of recent and rapid deformation (San Vicino and Cingoli, Fig. 3f). Note that age overlaps could also relate to the fact that LPS and fold growth may slightly overlap, as documented in the Sibillini thrust anticline, i.e. the southern continuation of the San Vicino anticline (Tavani et al., 2012).

In the four investigated anticlines, fold growth lasted between 1.5 and 15 Ma, in accordance with previous estimates of fold growth duration elsewhere using either syntectonic sedimentation (Holl and Anastasio, 1993; Anastasio et al., 2017) or mechanical modelling (Yamato et al., 2011). Moreover, our study quantifies for the first time the duration of the contraction before and after fold growth. The results unexpectedly reveal that LPS and LSFT, which accommodate lower amounts of shortening than fold growth but which are associated with substantial – if not most of – small-scale rock damage, may have lasted much longer than fold growth itself. Such a trend could be key for the understanding of the history of foreland basins, including the mechanical evolution of strata and past fluid flow dynamics (Roure et al., 2005; Beaudoin et al., 2014).

Dating precisely the onset of LPS, whatever the technique used (U–Pb geochronology or absolute thermometry of calcite cements of mesostructures) is difficult because the entire range of vein ages may not be captured with certainty due to limited sampling. However, the onset of LPS can be further constrained either by the sedimentary record of the foreland flexure preceding contraction (San Vicino) or by the estimate of the time at which compaction-related pressure solution along sedimentary stylolites is halted in the rocks in response to the switch of $\sigma 1$ axis from vertical to horizontal (Cingoli). The end of LSFT is also difficult to constrain precisely, but an upper bound is given by the change from fold-related shortening to a new regional state of stress. The latter is illustrated by the onset of post-orogenic extension in eastern UMAR (Fig. 3), by the late Pyrenean compression in the Pico del Aguila area (Fig. 5), and by the Basin and Range extension in the Laramide province (Fig. 6).

The four examples of folds also show that the overall duration of the folding event is variable (Fig. 7). Fold growth lasted longer in the case of forced folding above a high-angle basement thrust (Sheep Mountain) compared to fault-bend folding (San Vicino and Cingoli) along a flat-ramp decollement and detachment folding (Pico del Aguila) above a weak detachment layer in the cover (Fig. 7). The rapid fold growth and the relatively short LSFT in San Vicino and Cingoli are in line with the high rates of contraction and migration of deformation in the Apennines (Calamita et al., 1994, Fig. 7). In contrast, LSFT appears to last longer when folding is anchored to a high-angle basement thrust or when the fold is located at the front of the orogenic wedge, i.e. when the later propagation of deformation is limited or slow or when it occurs in a complex sequence (Pico del Aguila and Sheep Mountain, Fig. 7). The duration of LPS reflects to some degree the duration of the stress/strain accumulation in rocks required to generate folding, which can depend on the structural style (Beaudoin et al., 2020c). Our results support that a longer LPS (and a higher level of differential stress as well) is required to cause the inversion of a high-angle basement normal fault and related forced folding of the undetached

sedimentary cover (Sheep Mountain) than to initiate folding of the cover above a weak decollement (Pico del Aguila, Cingoli and San Vicino, Fig. 7). The longer LPS at Pico del Aguila with respect to San Vicino and Cingoli (Fig. 7) likely reflects the longer accumulation of displacement required to initiate folding oblique to the regional compression rather than perpendicular to it. It is worth noting that at first glance the fracture pattern (e.g. Tavani et al., 2015) remains basically similar whatever the overall duration of the folding event and related deformation stages.

In summary, beyond regional implications, this study demonstrates that pre-, syn-, and post-tilting mesostructures that formed under the same contraction as folding can be successfully dated. Our results bring for the first time absolute time constraints on the age and duration of the entire folding event for several upper-crustal folds formed in different contractional settings. In particular, we not only better constrain the age and duration of the fold growth stage but also the onset and duration of the layer-parallel shortening stage that predates folding and the duration and end of the late-stage fold tightening. Because the duration of each deformation stage is found to depend on the structural style and/or the regional sequence of deformation, our results emphasize the need to more carefully consider the entire folding event for a better appraisal of folding processes and stress/strain evolution in orogenic forelands and for a more accurate prediction of host rock damage and fluid migrations in naturally fractured reservoirs within folded domains.

Data availability. Data are either available in the Supplement or come from properly cited literature (Sect. 3).

Supplement. The supplement related to this article is available online at: https://doi.org/10.5194/se-12-2145-2021-supplement.

Author contributions. Conceptualization was carried out by OL and NEB. Data acquisition was done by all authors. Vizualization was carried out by OL, NEB, GH, and AL. NEB was responsible for funding acquisition. NEB and OL prepared the original draft of the paper. OL, NEB, GH, JPC reviewed and edited the paper.

Competing interests. The contact author has declared that neither they nor their co-authors have any competing interests.

Disclaimer. Publisher's note: Copernicus Publications remains neutral with regard to jurisdictional claims in published maps and institutional affiliations.

Acknowledgements. The authors would like to thank the two anonymous reviewers for their constructive comments, as well as Fabrizio Storti, Catherine Mottram, and Stephen Marshak for their comments on an earlier version of the paper. The authors also thank topical editor Virginia Toy for editorial handling.

Financial support. Nicolas Beaudoin is funded through the ISITE programme E2S, supported by ANR PIA and Region Nouvelle-Aquitaine.

Review statement. This paper was edited by Virginia Toy and reviewed by two anonymous referees.

References

Ahmadhadi, F., Daniel, J. M., Azzizadeh, M., and Lacombe, O.: Evidence for pre-folding vein development in the Oligo-Miocene Asmari Formation in the Central Zagros Fold Belt, Iran, Tectonics, 27, TC1016, https://doi.org/10.1029/2006TC001978, 2008.

Amrouch, K., Lacombe, O., Bellahsen, N., Daniel, J. M., and Callot, J. P.: Stress and strain patterns, kinematics and deformation mechanisms in a basement-cored anticline: Sheep Mountain Anticline, Wyoming, Tectonics, 29, TC1005, https://doi.org/10.1029/2009TC002525, 2010a.

Amrouch, K., Robion, P., Callot, J. P., Lacombe, O., Daniel, J. M., Bellahsen, N., and Faure, J. L.: Constraints on deformation mechanisms during folding provided by rock physical properties: a case study at Sheep Mountain anticline (Wyoming, USA), Geophys. J. Int., 182, 1105–1123, 2010b.

Amrouch, K., Beaudoin, N., Lacombe, O., Bellahsen, N., and Daniel, J. M.: Paleostress magnitudes in folded sedimentary rocks, Geophys. Res. Lett., 38, L17301, https://doi.org/10.1029/2011GL048649, 2011.

Anastasio, D., Kodama, K., and Parés, J.: Episodic deformation rates recovered from growth strata, Pyrenees, Search and Discovery, AAPG Datapages/Search and Discovery Article #90291, AAPG Annual Convention and Exhibition, Houston, Texas, 2–5 April 2017, 30553, 2017.

Aubourg, C., Smith, B., Eshraghi, A., Lacombe, O., Authemayou, C., Amrouch, K., Bellier O., and Mouthereau, F.: New magnetic fabric data and their comparison with palaeostress markers in the Western Fars Arc (Zagros, Iran): tectonic implications, Geol. Soc. Sp., 330, 97–120, 2010.

Barbier, M., Leprêtre, R., Callot, J. P., Gasparrini, M., Daniel, J. M., Hamon, Y., Lacombe O., and Floquet, M.: Impact of fracture stratigraphy on the paleo-hydrogeology of the Madison Limestone in two basement-involved folds in the Bighorn basin (Wyoming, USA), Tectonophysics, 576, 116–132, 2012.

Barchi, M.: The Neogene–Quaternary evolution of the Northern Apennines: crustal structure, style of deformation and seismicity, J. Virtual Explor., 36, 11, https://doi.org/10.3809/jvirtex.2010.00220, 2010.

Barnes P. M.: Active folding of Pleistocene unconformities on the edge of the Australian–Pacific plate boundary zone, offshore North Canterburry, New Zealand, Tectonics, 15, 623–640, 1996.

Beaudoin, N., Leprêtre, R., Bellahsen, N., Lacombe, O., Amrouch, K., Callot, J. P., Emmanuel, L., and Daniel, J. M.: Structural and microstructural evolution of the Rattlesnake Mountain Anticline

(Wyoming, USA): New insights into the Sevier and Laramide orogenic stress build-up in the Bighorn Basin, Tectonophysics, 576–577, 20–45, 2012.

Beaudoin, N., Bellahsen, N., Lacombe, O., Emmanuel, L., and Pironon, J.: Crustal-scale fluid flow during the tectonic evolution of the Bighorn Basin (Wyoming, USA), Basin Res., 26, 403–435, 2014.

Beaudoin, N., Huyghe, D., Bellahsen, N., Lacombe, O., Emmanuel, L., Mouthereau, F., and Ouahnon, L.: Fluid systems and fracture development during syn-depositional fold growth: example from the Pico del Aguila Anticline, Sierras Exteriores, Southern Pyrenees, Spain, J. Struct. Geol., 70, 23–38, 2015.

Beaudoin, N., Koehn, D., Lacombe, O., Lecouty, A., Billi, A., Aharonov, E., and Parlangeau, C.: Fingerprinting stress: Stylolite and calcite twinning paleopiezometry revealing the complexity of progressive stress patterns during folding-The case of the Monte Nero anticline in the Apennines, Italy, Tectonics, 35, 1687–1712, 2016.

Beaudoin, N., Lacombe, O., Roberts, N. M. W., and Koehn, D.: U–Pb dating of calcite veins reveals complex stress evolution and thrust sequence in the Bighorn Basin, Wyoming, USA, Geology, 46, 1015–1018, 2018.

Beaudoin, N., Gasparrini, M., David, M. E., Lacombe, O., and Koehn, D.: Bedding-parallel stylolites as a tool to unravel maximum burial depth in sedimentary basins: application to Middle Jurassic carbonate reservoirs in the Paris basin, France, Geol. Soc. Am. Bull., 131, 1239–1254, 2019.

Beaudoin N. E., Lacombe, O., Koehn, D., David, M. E., Farrell, N., and Healy, D.: Vertical stress history and paleoburial in foreland basins unravelled by stylolite roughness paleopiezometry: Insights from bedding-parallel stylolites in the Bighorn Basin, Wyoming, USA, J. Struct. Geol., 136, 104061, https://doi.org/10.1016/j.jsg.2020.104061, 2020a.

Beaudoin, N., Labeur, A., Lacombe, O., Koehn, D., Billi, A., Hoareau, G., Boyce, A., John, C. M., Marchegiano, M., Roberts, N. M., Millar, I. L., Claverie, F., Pecheyran, C., and Callot, J. P.: Regional-scale paleofluid system across the Tuscan Nappe–Umbria Marche Apennine Ridge (northern Apennines) as revealed by mesostructural and isotopic analyses of stylolite-vein networks, Solid Earth, 11, 1617–1641, 2020b.

Beaudoin, N., Lacombe, O., David, M. E., and Koehn, D.: Does stress transmission in forelands depend on structural style? Distinctive stress magnitudes during Sevier thin-skinned and Laramide thick-skinned layer-parallel shortening in the Bighorn Basin (USA) revealed by stylolite and calcite twinning paleopiezometry, Terra Nova, 32, 225–233, 2020c.

Bellahsen, N., Fiore, P., and Pollard, D. D.: The role of fractures in the structural interpretation of Sheep Mountain Anticline, Wyoming, J. Struct. Geol., 28, 850–867, 2006.

Bertotti, G., de Graaf, S., Bisdom, K., Oskam, B., Vonhof, H. B., Bezerra, F. H. R., Reijmer, J. J. G., and Cazarin, C. L.: Fracturing and fluid-flow during post-rift subsidence in carbonates of the Jandaíra Formation, Potiguar Basin, NE Brazil, Basin Res., 29, 836–853, 2017.

Bons, P. D., Elburg, M. A., and Gomez-Rivas, E.: A review of the formation of tectonicveins and their microstructures, J. Struct. Geol., 43, 33–62, 2012.

Branellec, M., Callot, J. P., Nivière, B., and Ringenbach, J. C.: The fracture network, a proxy for mesoscale deformation: Constraints on layer parallel shortening history from the Malargüe fold and thrust belt, Argentina, Tectonics, 34, 623–647, 2015.

Butler, R. W. H. and Lickorish, W. H.: Using high-resolution stratigraphy to date fold and thrust activity: examples from the Neogene of south-central Sicily, J. Geol. Soc. London, 154, 633–643, 1997.

Calamita, F., Cello, G., Deiana, G., and Paltrinieri, W.: Structural styles, chronology rates of deformation, and time-space relationships in the Umbria–Marche thrust system (central Apennines, Italy), Tectonics, 13, 873–881, 1994.

Callot, J. P., Robion, P., Sassi, W., Guiton, M. L. E., Kallel, N., Daniel, J. M., Mengus, J. M., and Schmitz, J.: Magnetic characterisation of folded aeolian sandstones: interpretation of magnetic fabric in diamagnetic rocks, Tectonophysics, 495, 230–245, 2010.

Camp, V. E., Pierce, K. L., and Morgan, L. A.: Yellowstone plume trigger for Basin and Range extension, and coeval emplacement of the Nevada–Columbia Basin magmatic belt, Geosphere, 1, 203–225, 2015.

Caricchi, C., Aldega, L., and Corrado, S.: Reconstruction of maximum burial along the Northern Apennines thrust wedge (Italy) by indicators of thermal exposure and modeling, Geol. Soc. Am. Bull., 127, 428–442, 2015.

Carrigan, J. H., Anastasio D. J., Kodama K. P., and Parés J. M.: Fault-related fold kinematics recorded by terrestrial growth strata, Sant Llorenç de Morunys, Pyrenees Mountains, NE Spain, J. Struct. Geol., 91, 161–176, 2016.

Craddock, J. P., Jackson, M., van der Pluijm, B. A., and Versical, R. T.: Regional shortening fabrics in eastern North America: Far-field stress transmission from the Appalachian–Ouachita Orogenic Belt, Tectonics, 12, 257–264, 1993.

Cruset, D., Vergés, J., Albert, R., Gerdes, A., Benedicto, A., Cantarero, I., and Travé, A.: Quantifying deformation processes in the SE Pyrenees using U–Pb dating of fracture-filling calcites, J. Geol. Soc. London, 177, 1186–1196, 2020.

Cruset, D., Vergés, J., Rodrigues, N., Belenguer, J., Pascual-Cebrian, E., Almar, Y., Perez-Caceres I., Macchiavelli C., Trave A., Beranoaguirre A., Albert R., Gerdes A., and Messager, G.: U–Pb dating of carbonate veins constraining timing of beef growth and oil generation within Vaca Muerta Formation and compression history in the Neuquén Basin along the Andean fold and thrust belt, Mar. Petrol. Geol., 132, 105204, https://doi.org/10.1016/j.marpetgeo.2021.105204, 2021.

Curzi, M., Aldega, L., Bernasconi, S. M., Berra, F., Billi, A., Boschi, C., Franchini S., Van der Lelij R, Viola G., and Carminati, E.: Architecture and evolution of an extensionally-inverted thrust (Mt. Tancia Thrust, Central Apennines): Geological, structural, geochemical, and K–Ar geochronological constraints, J. Struct. Geol., 136, 104059, https://doi.org/10.1016/j.jsg.2020.104059, 2020.

Ebner, M., Koehn, D., Toussaint, R., Renard, F., and Schmittbuhl, J.: Stress sensitivity of stylolite morphology, Earth Planet. Sc. Let., 277, 394–398, 2009.

Evans, M. A. and Fischer, M. P.: On the distribution of fluids in folds: A review of controlling factors and processes, J. Struct. Geol., 44, 2–24, 2012.

Grobe, A., von Hagke, C., Littke, R., Dunkl, I., Wübbeler F., Muchez P., and Urai, J. L.: Tectono-thermal evolution of Oman's Mesozoic passive continental margin under the obducting Semail

Ophiolite: a case study of Jebel Akhdar, Oman, Solid Earth, 10, 149–175, 2019.

Guiton M. L., Sassi W., Leroy Y., and Gauthier B. D.: Mechanical constraints on the chronology of fracture activation in folded Devonian sandstones of the western Moroccal Anti-Atlas, J. Struct. Geol., 25, 1317–1330, 2003.

Hansman, R. J., Albert, R., Gerdes, A., and Ring, U.: Absolute ages of multiple generations of brittle structures by U–Pb dating of calcite, Geology, 46, 207–210, 2018.

Hnat, J. S. and van der Pluijm, B. A.: Foreland signature of indenter tectonics: Insights from calcite twinning analysis in the Tennessee salient of the Southern Appalachians, USA, Lithosphere, 3, 317–327, 2011.

Hoareau, G., Crognier, N., Lacroix, B., Aubourg, C., Roberts, N. W., Niemi, N., Branellec, M., Beaudoin, N. E., and Suárez Ruiz, I.: Combination of Δ47 and U–Pb dating in tectonic calcite veins unravel the last pulses related to the Pyrenean Shortening (Spain), Earth Planet. Sc. Let., 553, 116636, https://doi.org/10.1016/j.epsl.2020.116636, 2021.

Hogan, P. J. and Burbank, D. W.: Evolution of the Jaca piggyback basin and emergence of the external Sierras, southern Pyrenees, in: Tertiary Basins of Spain, edited by: Friend, P. F. and Dabrio, C. J., Cambridge Univ. Press, Cambridge, 153–160, 1996.

Holl, J. E. and Anastasio, D. J.: Paleomagnetically derived folding rates, southern Pyrenees, Spain, Geology, 21, 271–274, 1993.

Jolivet, M., Labaume, P., Monie, P., Brunel, M., Arnaud, N., and Campani, M.: Thermochronology constraints for the propagation sequence of the south Pyrenean basement thrust system (France–Spain), Tectonics 26, TC5007, https://doi.org/10.1029/2006TC002080, 2007.

Labeur, A., Beaudoin, N. E., Lacombe, O., Emmanuel, L., Petracchini, L., Daëron, M., Klimowicz, S., and Callot, J.-P.: Burial-deformation history of folded rocks unraveled by fracture analysis, stylolite paleopiezometry and vein cement geochemistry: A case ctudy in the Cingoli Anticline (Umbria–Marche, Northern Apennines), Geosciences, 11, 135, https://doi.org/10.3390/geosciences11030135, 2021.

Lacombe, O.: Calcite twins, a tool for tectonic studies in thrust belts and stable orogenic forelands, Oil Gas Sci. Technol., 65, 809–838, 2010.

Lacombe, O., Amrouch, K., Mouthereau, F., and Dissez, L.: Calcite twinning constraints on late Neogene stress patterns and deformation mechanisms in the active Zagros collision belt, Geology, 35, 263–266, 2007.

Lacombe, O., Malandain, J., Vilasi, N., Amrouch, K., and Roure, F.: From paleostresses to paleoburial in fold–thrust belts: preliminary results from calcite twin analysis in the Outer Albanides, Tectonophysics 475, 128–141, 2009.

Lacombe, O., Bellahsen, N., and Mouthereau, F.: Fracture patterns in the Zagros Simply Folded Belt (Fars, Iran): constraints on early collisional tectonic history and role of basement faults, Geol. Mag., 148, 940–963, 2011.

Lacombe, O., Tavani, S., and Soto, R.: Into the deformation history of folded rocks, Special Issue, Tectonophysics, 576–577, 1–3, 2012.

Masaferro, J. L., Bulnes, M., Poblet, J., and Eberli, G. P.: Episodic folding inferred from syntectonic carbonate sedimentation: the Santaren anticline, Bahamas foreland, Sediment. Geol., 146, 11–24, 2002.

Mazzoli, S., Deiana, G., Galdenzi, S., and Cello, G.: Miocene fault-controlled sedimentation and thrust propagation in the previously faulted external zones of the Umbria–Marche Apennines, Italy, EGU Stephan Mueller Special Publication Series, 1, 195–209, 2002.

Mottram, C. M., Parrish, R. R., Regis, D., Warren, C. J., Argles, T. W., Harris, N. B., and Roberts, N. M.: Using U–Th–Pb petrochronology to determine rates of ductile thrusting: Time windows into the Main Central Thrust, Sikkim Himalaya, Tectonics, 34, 1355–1374, 2015.

Mueller, K. and Suppe, J.: Growth of Wheeler Ridge anticline, California: geomorphic evidence for fault-bend folding behavior during earthquakes, J. Struct. Geol., 19, 383–396, 1997.

Nuriel P., Weinberger R., Kylander-Clark A. R. C., Hacker B. R., and Craddock J. P.: The onset of the Dead Sea transform based on calcite age-strain analyses, Geology, 45, 587–590, 2017.

Poblet, J. and Hardy, S.: Reverse modelling of detachment folds; application to the Pico del Aguila anticline in the south-central Pyrenees (Spain), J. Struct. Geol., 17, 1707–1724, 1995.

Poblet, J., McClay, K., Storti, F., and Munoz, J. A.: Geometry of syntectonic sediments associated with single-layer detachment folds, J. Struct. Geol., 19, 369–381, 1997.

Pueyo, E. L., Millan, H., and Pocoví, A.: Rotation velocity of a thrust: a paleomagnetic study in the External Sierras (Southern Pyrenees), Sediment. Geol., 146, 191–208, 2002.

Riba, O.: Syntectonic unconformities of the Alto Cardener, Spanish Pyrenees: A genetic interpretation, Sediment. Geol., 15, 213–233, 1976.

Roberts, N. M. and Walker, R. J.: U–Pb geochronology of calcite-mineralized faults: Absolute timing of rift-related fault events on the northeast Atlantic margin, Geology, 44, 531–534, 2016.

Roberts, N. M., Žák, J., Vacek, F., and Sláma, J.: No more blind dates with calcite: Fluid-flow vs. fault-slip along the Očkov thrust, Prague Basin, Geosci. Front., 12, 101143, https://doi.org/10.1016/j.gsf.2021.101143, 2021.

Roberts, N. M. W., Drost, K., Horstwood, M. S. A., Condon, D. J., Chew, D., Drake, H., Milodowski, A. E., McLean, N. M., Smye, A. J., Walker, R. J., Haslam, R., Hodson, K., Imber, J., Beaudoin, N., and Lee, J. K.: Laser ablation inductively coupled plasma mass spectrometry (LA-ICP-MS) U–Pb carbonate geochronology: strategies, progress, and limitations, Geochronology, 2, 33–61, 2020.

Rocher, M., Lacombe, O., Angelier, J., and Chen H. W.: Mechanical twin sets in calcite as markers of recent collisional events in a fold-and-thrust belt: evidence from the reefal limestones of southwestern Taiwan, Tectonics 15, 984–996, 1996.

Rocher, M., Lacombe, O., Angelier, J., Deffontaines, B., and Verdier, F.: Cenozoic folding and faulting in the south Aquitaine Basin (France): insights from combined structural and paleostress analyses, J. Struct. Geol., 22, 627–645, 2000.

Rolland, A., Toussaint, R., Baud, P., Schmittbuhl, J., Conil, N., Koehn, D., Renard, F., and Gratier, J.-P.: Modeling the growth of stylolites in sedimentary rocks, J. Geophys. Res., 117, B06403, https://doi.org/10.1029/2011JB009065, 2012.

Rolland, A., Toussaint, R., Baud, P., Conil, N., and Landrein, P.: Morphological analysis of stylolites for paleostress estimation in limestones, Int. J. Rock Mech. Min. Sci., 67, 212–225, https://doi.org/10.1016/j.ijrmms.2013.08.021, 2014.

Roure, F., Swennen, R., Schneider, F., Faure, J. L., Ferket, H., Guilhaumou, N., Osadetz, K., Robion, P., and Vandeginste, V.: Incidence and Importance of Tectonics and Natural Fluid Migration on Reservoir Evolution in Foreland Fold-And-Thrust Belts, Oil Gas Sci. Technol., 60, 67–106, 2005.

Sassi, W., Guiton, M., Leroy, Y. M., Kallel, N., Callot, J. P., Daniel, J. M., Lerat, O., and Faure, J. L.: Constraints on mechanical modelling of folding provided by matrix deformation and fracture network analysis: The case of Split Mountain (Utah, USA), Tectonophysics, 576–577, 197–215, 2012.

Schmittbuhl, J., Renard, F., Gratier, J. P., and Toussaint, R.: Roughness of stylolites: implications of 3D high resolution topography measurements, Phys. Rev. Lett., 93, 238501, https://doi.org/10.1103/PhysRevLett.93.238501, 2004.

Schneider, S., Hammerschmidt, K., and Rosenberg, C. L.: Dating the longevity of ductile shear zones: Insight from 40Ar/39Ar in situ analyses, Earth Planet. Sc. Let., 369, 43–58, 2013.

Shackleton, J. R., Cooke, M. L., Verges, J., and Sima, T.: Temporal constraints on fracturing associated with fault-related folding at Sant Corneli anticline, Spanish Pyrenees, J. Struct. Geol., 33, 5–19, 2011.

Storti, F. and Poblet, J.: Growth stratal architectures associated to decollement folds and fault-propagation folds. Inferences on fold kinematics, Tectonophysics, 282, 353–373, 1997.

Suppe, J., Chou, G. T., and Hook, S. C.: Rates of folding and faulting determined from growth strata, in: Thrust Tectonics, edited by: McClay, K. R., Chapman & Hall, Suffolk, 105–121, 1992.

Tavani, S., Storti, F., Fernández, O., Muñoz, J. A., and Salvini, F.: 3-D deformation pattern analysis and evolution of the Añisclo anticline, southern Pyrenees, J. Struct. Geol., 28, 695–712, 2006.

Tavani, S., Storti, F., Salvini F., and Toscano C.: Stratigraphic versus structural control on the deformation pattern associated with the evolution of the Mt. Catria anticline, Italy, J. Struct. Geol., 30, 664–681, 2008.

Tavani, S., Mencos, J., Bausà, J., and Muñoz, J. A.: The fracture pattern of the Sant Corneli Bóixols oblique inversion anticline (Spanish Pyrenees), J. Struct. Geol., 33, 1662–1680, 2011.

Tavani, S., Storti, F., Bausa, J., and Munoz, J. A.: Late thrusting extensional collapse at the mountain front of the northern Apennines (Italy), Tectonics, 31, TC4019, https://doi.org/10.1029/2011TC003059, 2012.

Tavani, S., Storti, F., Lacombe, O., Corradetti, A., Muñoz, J., and Mazzoli, S.: A review of deformation pattern templates in foreland basin systems and fold-and-thrust belts: Implications for the state of stress in the frontal regions of thrust wedges, Earth-Sci. Rev., 141, 82–104, 2015.

Toussaint, R., Aharonov, E., Koehn, D., Gratier, J. P., Ebner, M., Baud, P., Rolland, A., and Renard, F.: Stylolites: A review, J. Struct. Geol., 114, 163–195, 2018.

Varga, R. J.: Rocky Mountain foreland uplifts: products of a rotating stress field or strain partitioning?, Geology, 21, 1115–1118, 1993.

Vermeesch, P.: Unifying the U–Pb and Th–Pb methods: joint isochron regression and common Pb correction, Geochronology, 2, 119–131, 2020.

Vidal-Royo, O., Koyi, H. A., and Muñoz, J. A.: Formation of orogen-perpendicular thrusts due to mechanical contrasts in the basal décollement in the Central External Sierras (Southern Pyrenees, Spain), J. Struct. Geol., 31, 523–539, 2009.

Weil, A. B. and Yonkee, W. A.: Layer-parallel shortening across the Sevier fold-thrust belt and Laramide foreland of Wyoming: spatial and temporal evolution of a complex geodynamic system, Earth Planet. Sc. Let., 357–358, 405–420, 2012.

Yamato, P., Kaus, B. J., Mouthereau, F., and Castelltort, S.: Dynamic constraints on the crustal-scale rheology of the Zagros fold belt, Iran, Geology, 39, 815–818, 2011.

Wang, Y., Zwingmann, H., Zhou, L., Lo, C.-H., Viola, G., and Hao, J.: Direct dating of folding events by 40Ar/39Ar analysis of synkinematic muscovite from flexural-slip planes, J. Struct. Geol., 83, 46–59, 2016.